Extended Nucleation of the 1999 M_W 7.6 Izmit Earthquake

Michel Bouchon *et al.*

Science **331**, 877 (2011);
DOI: 10.1126/science.1197341

Extended Nucleation of the 1999 M_w 7.6 Izmit Earthquake

Michel Bouchon,[1]* Hayrullah Karabulut,[2] Mustafa Aktar,[2] Serdar Özalaybey,[3] Jean Schmittbuhl,[4] Marie-Paule Bouin[5]

Laboratory and theoretical studies suggest that earthquakes are preceded by a phase of developing slip instability in which the fault slips slowly before accelerating to dynamic rupture. We report here that one of the best-recorded large earthquakes to date, the 1999 moment magnitude (M_w) 7.6 Izmit (Turkey) earthquake, was preceded by a seismic signal of long duration that originated from the hypocenter. The signal consisted of a succession of repetitive seismic bursts, accelerating with time, and increased low-frequency seismic noise. These observations show that the earthquake was preceded for 44 minutes by a phase of slow slip occurring at the base of the brittle crust. This slip accelerated slowly initially, and then rapidly accelerated in the 2 minutes preceding the earthquake.

The existence or observation of a detectable nucleation phase before earthquakes is a long-standing goal with implications for earthquake prediction and risk assessment. Although it is well established that some earthquakes are preceded by foreshocks, nothing so far distinguishes these foreshocks from regular earthquake occurrences, so there is no objective way to identify these events as foreshocks until they are followed by a larger earthquake (*1*). On the other hand, the presence of a short-duration (a few seconds or less) nucleation phase on some earthquake records, which would indicate the growth of slip instability on the fault before the earthquake, has been strongly debated (*2*). Laboratory (*3*–*6*) and theoretical (*7*–*14*) models of earthquake nucleation predict that slip instability should occur before earthquakes, but whether that instability is large enough to be detected in real Earth conditions and of long enough duration to be helpful is unknown (*15*). In this context, we examined the seismic signal preceding the 1999 Izmit earthquake, the largest well-recorded strike-slip earthquake to date, to characterize any existing nucleation phase.

The earthquake. The Izmit earthquake occurred at 0 hours, 1 min, 38 s (00h01mn38s; universal time) on 17 August 1999 and, in ~25 s, broke the North Anatolian fault, a major plate boundary, over a length of 150 km across northwestern Turkey (*16*–*19*). During the earthquake, the two plates bounding the fault moved horizontally past each other by ~3 m. This sudden motion of the plates occurred over the brittle part of the crust, which in this region extends from Earth's surface to a depth of ~17 km (*20*). Below, rocks are more ductile because of the increase in temperature, and the two plates move continuously past each other by ~2.5 cm per year (*21*). What happens in the transition zone between the brittle and the ductile parts of the crust—possibly including the occurrence of nonvolcanic tremor—may influence the nucleation of the large earthquakes but is largely unknown.

Estimates of the depth of the hypocenter vary slightly (*16*, *20*), but are all comprised in the range 15 ± 2 km, which places the zone of nucleation near the base of the brittle crust. The earthquake was preceded by foreshocks (*20*, *22*), the largest one being reported by two local seismic stations (*20*, *22*). The station closest to the epicenter (located 14 km away) reported the occurrence of seven other foreshocks (*20*). This station (UCG; fig. S1) was equipped with a short-period (1 Hz, L4C) seismometer with a vertical component, coupled with a digital recorder (*23*). This instrument recorded the vertical velocity of the ground at a sampling rate of 100 Hz. Its records shed some light on the mechanical processes taking place in the hypocentral area of a large earthquake before the earthquake occurs.

Nucleation signal. Station UCG was located on limestone, a hard rock which does not substantially attenuate or affect seismic waves and thus provides good recording conditions. It was operated in triggered mode like many seismic stations, meaning that it recorded only when a preset threshold of ground-motion amplitude was exceeded (*24*). In all, the ground motion was recorded in six triggered windows during the 45 min preceding the earthquake, providing almost 10 min (563 s) of records. In one of these recordings, 20 min before the earthquake, five shocks are visible (Fig. 1). Each one begins with a *P*-wave sequence followed 2.4 s later by higher-amplitude *S* waves. Some of the shocks occur less than 5 s apart. A total of 18 events, ranging in magnitude from 0.3 to 2.7 (table S1), can be visually identified in the six triggered windows (Fig. 2). Two characteristics of these shocks stand out: Their *S*-minus-*P* travel times are the same, within the digitization precision (0.01 s), and their waveforms are surprisingly similar, in spite of the wide range of magnitude they cover.

Several other stations, located in various azimuths from the epicenter, also recorded the largest foreshock. At the closest station other than UCG (fig. S1), the *P*-wave arrival is clear so that the time difference between the largest foreshock and the main shock can be measured accurately. This time difference (105.22 s) is exactly the same, within the digitization precision (0.01 s), as the one measured at UCG, which shows that the travel times of the *P*-wave from the foreshock and from the main shock hypocenter to the stations are the same and implies that the source of the foreshocks is the hypocenter. Furthermore, at all of the stations where the largest foreshock was recorded, *P*-wave polarity is the same as the main shock, indicating that the slip mechanism of the foreshocks is the same as the main shock.

Because all of the events share nearly the same waveform, the waveform of one of them

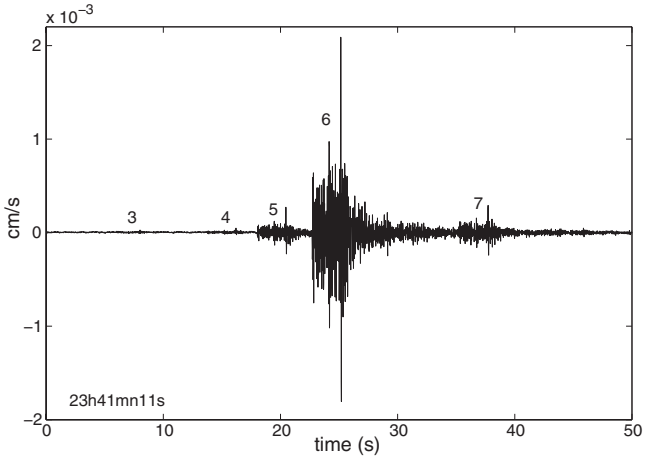

Fig. 1. Record of the vertical ground motion 20 min before the earthquake. This recording is part of the second triggered window. The numbers indicate the foreshocks and refer to their chronological order from the start of the sequence.

[1]Centre National de la Recherche Scientifique and Université Joseph Fourier, Grenoble, ISTerre, BP 53, 38041 Grenoble, France. [2]Kandilli Observatory and Earthquake Research Institute, Bogaziçi University, 81220 Cengelköy, Istanbul, Turkey. [3]TÜBITAK, Marmara Research Center, Earth and Marine Sciences Institute, 41470 Gebze, Kocaeli, Turkey. [4]Centre National de la Recherche Scientifique and Université de Strasbourg, Ecole et Observatoire des Sciences de la Terre, 5 rue Descartes, 67084 Strasbourg, France. [5]Centre National de la Recherche Scientifique and Institut de Physique du Globe de Paris, Observatoire Volcanologique et Sismologique de Guadeloupe, 97113 Gourbeyre, Guadeloupe, France.

*To whom correspondence should be addressed. E-mail: Michel.Bouchon@ujf-grenoble.fr

may be used as a template to try to detect the presence of smaller shocks for which the signal is within the noise level. This is performed by cross-correlating the template with the records (*24*). As a result, many more events than the ones visually recognized can be detected (Fig. 3A), bringing the total number of identified events to about 40.

Interevent separation. To confirm that the events originate from the same or nearly the same place, we compared the first two events. Visually, their waveforms (Fig. 4A) are nearly the same. Cross-correlating them (Fig. 4B) yields a difference between the *S*-minus-*P* travel times of the two events of ~0.0006 s. This value, which is at the limit of the resolution of the measurement, implies a separation distance of ~5 m. Although this separation between the two events is the one seen from the station and is thus the projection of the real separation on the travel path of the waves, its value is surprisingly small compared with the size of the sources (*25*).

We extended this analysis by cross-correlating the *P* and *S* waves of all possible pairs of events (136, as the *P*-wave of foreshock 8, which is outside the triggered window, was not recorded) and calculating the difference in *S*-minus-*P* time for each pair. As the position and length of the windows selected for the correlation may affect the results (because of the presence of noise and the asymmetry of the pulse shapes), we considered 200 different windows for each event pair. The results show that any one of the events differs in *S*-minus-*P* travel time by less than 0.0024 s from the majority of the other events, regardless of the correlation windows that we considered. This implies that any one shock is located within 20 m or less from the majority of the other events. Although this separation is the one seen from the station, its small value, compared with the likely source size of the largest shocks (*25*), shows that all of the events originate from an area of the fault that is no larger than the size of the largest events.

Slip acceleration. Laboratory and theoretical studies suggest that earthquakes are preceded by a phase of developing slip instability in which the fault begins to slip slowly before accelerating to dynamic rupture (*3*–*14*). A correlation between the onset of slip acceleration and the emission of tremorlike signals has also been observed in friction experiments (*26*). If we consider only the largest events of the sequence, for which the detection should be complete because they are above the triggering threshold, we note that the fourth-largest event occurs 43 min before the earthquake, the third-largest one takes place 20 min before, the second-largest one 12 min before, and the largest one 1 min 45 s before the earthquake (Fig. 2 and table S1). The magnitudes of the fourth, third, and second events are relatively close, which suggests a slowly accelerating process in the first 42 min of the sequence, followed by a rapid acceleration 2 min before the earthquake. This rapid acceleration is also suggested by the occurrence of at least six shocks in the 40-s-long recording leading to the earthquake (Fig. 3A).

Less than 1 s before the earthquake, the process accelerated again, and the instability increased dramatically: One shock occurred 0.14 s before the earthquake, followed by another shock 0.07 s later, finally followed by the earthquake itself (Fig. 3B). In spite of the short time span between the first two shocks, the *P*-wave pulse of the first one can be clearly observed. Its shape and width are the same as the ones of the other events (Fig. 3B). A comparison of their amplitude shows that its magnitude is ~2.0. The shock that immediately follows has a broader *P* pulse and a higher amplitude than any of the previous shocks. The earthquake occurs 0.07 s later. More events or a

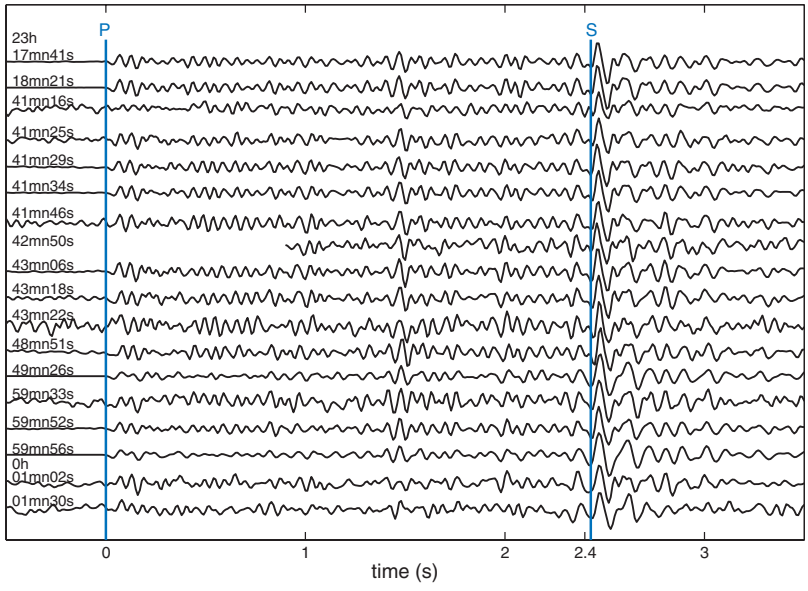

Fig. 2. Records of the foreshocks, arranged in chronological order from top to bottom. The starting time of each trace, the *P*-wave arrival, and the *S*-wave are indicated. Each trace is normalized to its peak amplitude, given in table S1. The origin of the time axis corresponds to the *P*-wave arrival.

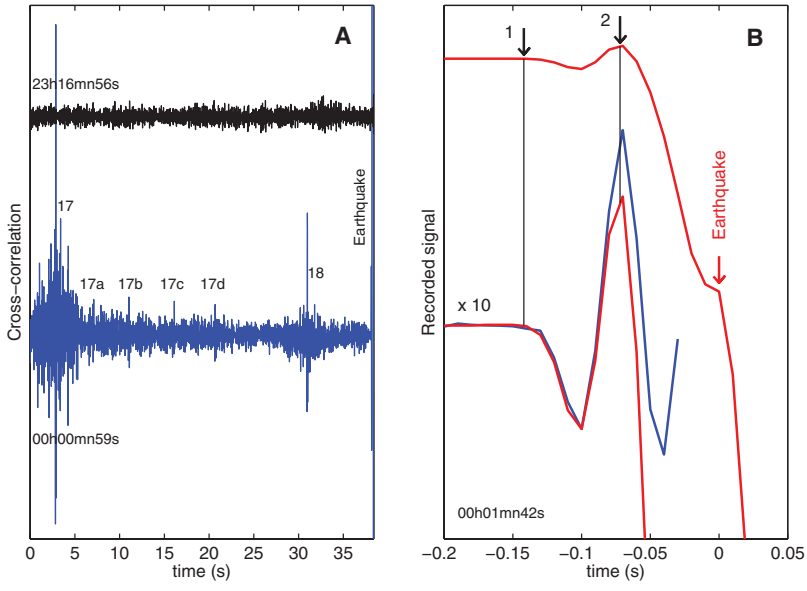

Fig. 3. (**A**) Signals obtained by cross-correlating the waveform of one of the foreshocks with the records. The top trace corresponds to the beginning of the first triggered window and occurs before the first foreshock. The bottom trace corresponds to the ground motion in the 40 s preceding the earthquake. Peaks in the correlation show the occurrence of several events with waveforms similar to the template. Numbers 17 and 18 refer to the chronological order of the foreshocks in Fig. 2. Peaks 17, a to d, are interpreted as four newly detected events. (**B**) Seismic signal immediately preceding the earthquake. The recorded ground motion (top trace) shows the occurrence of two shocks 0.14 and 0.07s before the earthquake. The lower red trace shows the first part of the same record amplified 10 times compared with the *P* waveform of the prior foreshocks (shown in blue, foreshock 2).

cascade of events may have occurred in the short time span leading to the earthquake, but the data resolution cannot distinguish anything else other than these two immediate foreshocks.

Repeating events? The seismic signal before the earthquake shows a repetitive pattern of events with the same waveform (Figs. 2 and 3). Events occurred at 40-s (in the first triggered window), ~10-s (on average), ~5-s, and then at tenths-of-a-second intervals.

The comparison of the spectra of the shocks (fig. S2) confirms the similarity observed in the waveforms. Most of the shocks have nearly the same spectral shape and corner frequencies (the frequency beyond which the spectral amplitude decays). This similitude is especially clear for some of the events (Fig. 5). In particular, the two strongest shocks have nearly identical spectral shapes (Fig. 5C). Considering these two shocks, two possible reasons may cause this similitude: (i) Their spectral corner frequencies are both higher than the maximum frequency displayed (35 Hz), which means that the two shocks appear as point sources over the frequency range considered and that their source size is not resolvable with the data. (ii) Alternatively, the two events may have nearly the same corner frequencies, because spectral amplitude drops off rapidly beyond an event corner frequency. The first hypothesis would imply an extremely high stress drop on the order of 800 MPa for the largest shock [based on the approach in (*27*)]. Such a high value lies well outside the range of values observed for tectonic earthquakes (*28*, *29*). Thus, it appears likely that the two events have similar corner frequencies. As corner frequency is inversely proportional to source dimension, it implies that their source size is nearly the same. This is surprising because the shocks have very different amplitudes (table S1).

An estimate of the source extent of these two shocks can be obtained by modeling their source as a patch of shear slip located at the hypocenter and matching the calculated spectral shape with the one observed. This yields a patch size of ~300 m (fig. S3). As the calculation does not account for the anelastic attenuation of the waves, which is not precisely known and might shift the spectral peak to lower frequency, this measurement should be considered as an upper limit of the source size. Regardless of its precise value, however, the similitude of the spectral shapes of the two events well beyond their spectral peak seems to require that their source size is nearly the same. The small separation distance of the two events, seen from the station and estimated from their waveform cross-correlation (~9 m), further supports the notion that the same patch is the source of the two events. The amplitude of the two shocks differs by a factor of 10, which implies that their stress drops (the release of stress on the source patch) also differ by a factor of 10. If the stress drop had been similar for the two shocks, their amplitude ratio would have implied a little more than a factor of 2 difference in their corner frequencies (seismic moment, which is the physical measure of an earthquake strength, scales as the cube of the source dimension). This is clearly not what we have observed (Fig. 5C). The source dimension inferred (fig. S3) implies that the slip on the patch is, on average, a little less than 1 cm (0.8 cm) for the largest shock and a little less than 1 mm (0.8 mm) for the other one. These values lead to a stress drop of ~2.6 MPa for the largest shock, a value typical for earthquakes, and ~0.3 MPa for the second event, a lower value than commonly observed.

The similarity of the spectra of the other shocks (figs. S2 and S4) is intriguing but is more

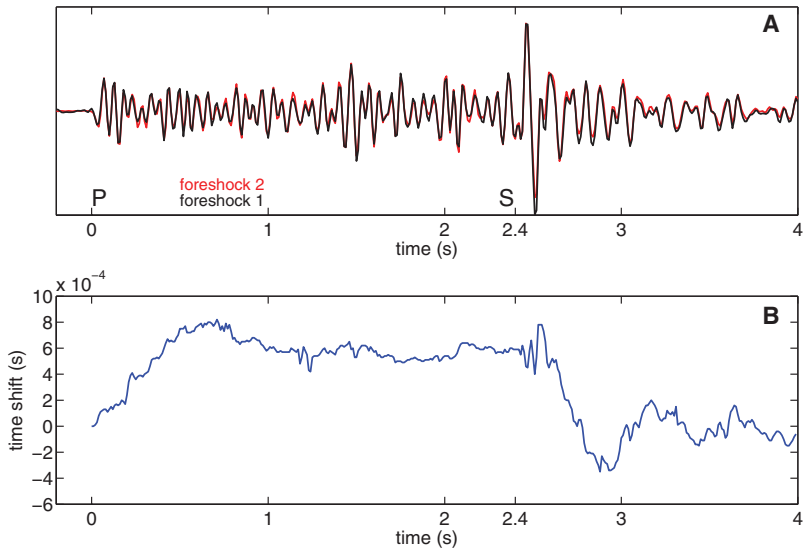

Fig. 4. (**A**) Superposition of the records of the first and second foreshocks. The second record has been shifted in time (in the Fourier domain) by the time increment that maximizes the cross-correlation of the two signals. The beginnings of the *P* and *S* waves are indicated. The *P* arrivals correspond to the origin of the time axis. The nonzero amplitude before the *P* arrivals shows the noise level of the records. (**B**) Evolution of the time shift that maximizes the correlation between the waveforms of the first two foreshocks. The correlation is done over a moving window 128 points long (1.28 s). The first window begins at the *P*-wave arrival and corresponds to the origin of the time axis. Subsequent time shifts are measured relative to this first window. The time shift is obtained by interpolating the correlation peak at each time step.

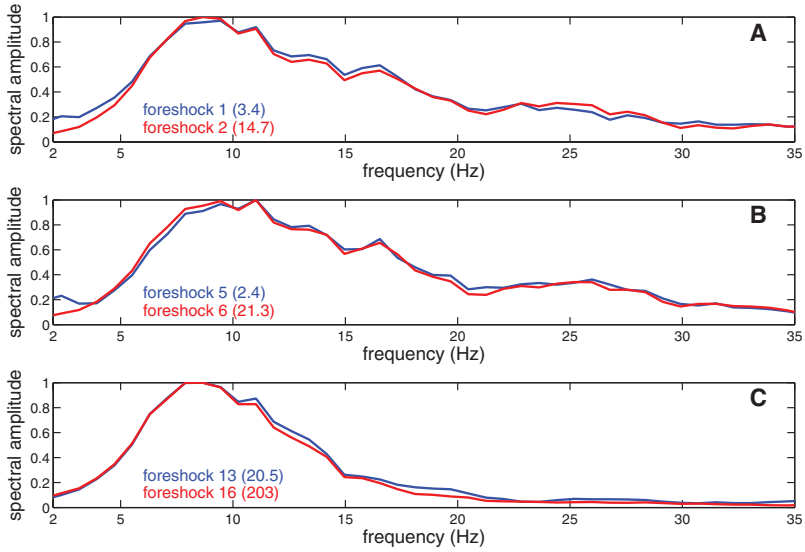

Fig. 5. (**A** to **C**) Comparison of the *S*-wave ground-velocity spectra of some events. Numbers refer to the chronological order of the foreshocks in Fig. 2. All of the spectra are corrected for the instrument response and normalized independently. Spectral amplitudes below 5 Hz are affected by the low-frequency background seismic noise, which scales differently from event to event. The peak recorded amplitude of each event is given in parenthesis and is expressed in micrometers per second. The two largest shocks are shown in (C).

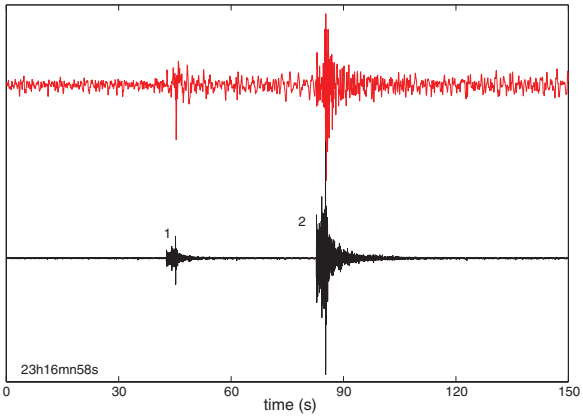

Fig. 6. Ground motion recorded in the first triggered window (bottom trace) and corresponding signal low-pass filtered below 3 Hz (top trace). Numbers indicate the first two foreshocks.

difficult to interpret. Either the relatively small magnitude of these events results in corner frequencies too high to be resolvable by the data, or all of these shocks have nearly the same source size, just slightly smaller than that of the two largest shocks. To make sure that this spectral similitude is not due to a local site effect at the station (such as a possible seismic resonance of the geological structure) or to anelastic attenuation along the travel path of the waves, we also present the spectra of some aftershocks, occurring a few days later and located at a comparable distance from the station (fig. S5). The wide range of spectral shapes that we observed suggests that the corner frequency of the shocks is not the result of a site or an attenuation effect, but is more likely a source effect. If this is the case, it would indicate that the pre-Izmit events have nearly the same source size. A consequence of this would be that the small events have extremely low stress drops, possibly comparable to the stress drops of the low-frequency earthquakes (*30*, *31*) that make up nonvolcanic tremor (*32*, *33*). Regardless of this possibility, the near duplicate spectrum of some of the events (Fig. 5, A and B) suggests that at least some repeating events occur, as is the case with the two strongest shocks.

Fault creep. As earthquakes are known to release stress on the part of the fault on which they occur, the presence of repeating events at few-minute (events 13 and 16, Fig. 5C) or possibly at few-second (events 5 and 6, Fig. 5B) intervals is intriguing. The repeating rupture of the same fault patch seems to require a reloading of stress on the patch between events. A simple mechanism that can provide this reloading is creep on the area surrounding the patch. Repeating events have been observed elsewhere, particularly on the San Andreas fault in California (*34*–*38*), and creep in the area surrounding the source is thought to be the cause. Compared with the present events, they usually have recurrent times of months or years and similar magnitudes. A possible reason for the magnitude difference observed here is that the interevent time of the pre-Izmit shocks is extremely short, possibly forcing the response of the patch. In other words, loading may be too fast to produce a steady response. Another possibility is that the patch responds not only to the loading but also to the loading rate, which may be highly irregular.

Another intriguing feature of the records is the change in the background low-frequency seismic noise that takes place after the first foreshock (Fig. 6). Coincidentally with the first foreshock, the low-frequency ground motion increases. Then, whereas the amplitude of the first foreshock decays rapidly after the *S*-wave arrival (bottom trace in Fig. 6), the low-frequency motion stays at a higher level than before the foreshock (top trace in Fig. 6). From then on, this low-frequency signal, which is also visible on the unfiltered records, was continuously present on all the recordings until the onset of the earthquake (fig. S6). Its spectrum shows that its frequency is below 2 Hz (fig. S7). Although it is not possible with one station to determine its origin, this low-frequency noise, whose beginning coincides with the occurrence of the first foreshock, may be the seismic signature of the fault creep that was then probably occurring around the hypocentral area.

Outlook. These observations show that this particular earthquake was preceded by a phase of slow slip occurring at the base of the brittle crust. The relatively long duration of the nucleation and the observation that it emits a characteristic signal are encouraging for possible early warning systems, but it remains to be seen whether this behavior is applicable to other large earthquakes. Some other well-recorded earthquakes, such as the 1999 Chi-Chi (Taiwan) or the 2004 Parkfield (California) earthquakes, do not show evidence for similar foreshocks or nucleation events. The next steps include reexamining the near-fault seismic records of other large, well-recorded earthquakes for similar signals. Continued seismic monitoring networks will also be necessary to understand if such extended nucleation events apply beyond this example.

References and Notes

1. C. H. Scholz, *The Mechanics of Earthquakes and Faulting* (Cambridge Univ. Press, Cambridge, 1990).
2. W. L. Ellsworth, G. C. Beroza, *Science* **268**, 851 (1995).
3. J. H. Dieterich, *J. Geophys. Res.* **83**, 3940 (1978).
4. J. H. Dieterich, *Tectonophysics* **211**, 115 (1992).
5. M. Ohnaka, *J. Phys. Earth* **41**, 45 (1993).
6. M. Ohnaka, L. F. Shen, *J. Geophys. Res.* **104**, 817 (1999).
7. S. Das, C. H. Scholz, *J. Geophys. Res.* **86**, 6039 (1981).
8. J. R. Rice, *J. Geophys. Res.* **98**, 9885 (1993).
9. B. Shibazaki, M. Matsu'ura, *Geophys. J. Int.* **132**, 14 (1998).
10. M. Campillo, P. Favreau, I. R. Ionescu, C. Voisin, *J. Geophys. Res.* **106**, 16307 (2001).
11. M. Cocco, A. Bizzarri, *Geophys. Res. Lett.* **29**, 1516 (2002).
12. P. Favreau, M. Campillo, I. R. Ionescu, *J. Geophys. Res.* **107**, 2147 (2002).
13. N. Lapusta, J. R. Rice, *J. Geophys. Res.* **108**, 2205 (2003).
14. J. P. Ampuero, A. M. Rubin, *J. Geophys. Res.* **113**, B01302 (2008).
15. R. E. Abercrombie, D. C. Agnew, F. K. Wyatt, *Bull. Seismol. Soc. Am.* **85**, 1873 (1995).
16. M. N. Toksöz, R. E. Reilinger, C. G. Doll, A. A. Barka, N. Yalcin, *Seismol. Res. Lett.* **70**, 669 (1999).
17. A. Barka *et al.*, *Bull. Seismol. Soc. Am.* **92**, 43 (2002).
18. M. Bouchon *et al.*, *Bull. Seismol. Soc. Am.* **92**, 256 (2002).
19. Z. Çakir *et al.*, *Geophys. J. Int.* **155**, 93 (2003).
20. S. Özalaybey *et al.*, *Bull. Seismol. Soc. Am.* **92**, 376 (2002).
21. R. Reilinger *et al.*, *J. Geophys. Res.* **111**, B05411 (2006).
22. O. Polat *et al.*, *Bull. Seismol. Soc. Am.* **92**, 361 (2002).
23. M. Aktar, F. Biçmen, *Cah. Cent. Eur. Géodyn. Sismol.* **1**, 11 (1989).
24. Materials and methods are available as supporting material on *Science* Online.
25. Assuming a stress drop of 3 MPa for the events, which is close to the average of the values commonly observed, and a circular source would lead to source dimension (diameter) of ~66 and 108 m for the first two foreshocks, respectively, and 290 m for the largest one.
26. D. Zigone, C. Voisin, E. Larose, F. Renard, M. Campillo, *Geophys. Res. Lett.* **38**, L01315 (2011).
27. R. Madariaga, *Bull. Seismol. Soc. Am.* **66**, 639 (1976).
28. R. E. Abercrombie, *J. Geophys. Res.* **100**, 24015 (1995).
29. K. Imanishi, W. L. Ellsworth, S. G. Prejean, *Geophys. Res. Lett.* **31**, L12S09 (2004).
30. S. Ide, G. C. Beroza, D. R. Shelly, T. Uchide, *Nature* **447**, 76 (2007).
31. G. C. Beroza, S. Ide, *Science* **324**, 1025 (2009).
32. D. R. Shelly, G. C. Beroza, S. Ide, S. Nakamula, *Nature* **442**, 188 (2006).
33. D. R. Shelly, G. C. Beroza, S. Ide, *Nature* **446**, 305 (2007).
34. J. E. Vidale, W. L. Ellsworth, A. Cole, C. Marone, *Nature* **368**, 624 (1994).
35. C. Marone, J. E. Vidale, W. L. Ellsworth, *Geophys. Res. Lett.* **22**, 3095 (1995).
36. D. P. Schaff, G. Beroza, B. E. Shaw, *Geophys. Res. Lett.* **25**, 4549 (1998).
37. R. M. Nadeau, T. V. McEvilly, *Science* **285**, 718 (1999).
38. O. Lengliné, D. Marsan, *J. Geophys. Res.* **114**, B10303 (2009).

39. We thank the TÜBITAK Marmara Research Center Earth and Marine Sciences Institute, specifically M. Ergin, C. Tapirdamaz, F. Biçmen, and A. Yörük, who participated in the operation of the seismic station and in the processing of the data. This study benefited from discussions with M. Campillo, O. Konca, D. Marsan, L. Géli, O. Lengliné, N. Toksöz, F. Renard, C. Voisin, P. Bernard, G. Poupinet, A. Paul, D. Zigone, V. Durand, A. M. Boullier, P. Henri, P. Y. Bard, O. Coutant, and H. Perfettini.

Supporting Online Material

www.sciencemag.org/cgi/content/full/331/6019/877/DC1
Materials and Methods
Figs. S1 to S7
Table S1
References

3 September 2010; accepted 13 January 2011
10.1126/science.1197341